Bifurcations and Chaos in Parametrically Excited Single-Degree-of-Freedom Systems

L. D. ZAVODNEY[1], A. H. NAYFEH[2] and N. E. SANCHEZ[3]

[1]*The Ohio State University, Department of Engineering Mechanics, Columbus, OH 43210, U.S.A.*
[2]*Virginia Polytechnic Institute and State University, Department of Engineering Science and Mechanics, Blacksburg, VA 24061, U.S.A.*
[3]*The University of Texas at San Antonio, Division of Engineering, San Antonio, TX 78285, U.S.A.*

Abstract. The behavior of single-degree-of-freedom systems possessing quadratic and cubic nonlinearities subject to parametric excitation is investigated. Both fundamental and principal parametric resonances are considered. A global bifurcation diagram in the excitation amplitude and excitation frequency domain is presented showing different possible stable steady-state solutions (attractors). Fractal basin maps for fundamental and principal parametric resonances when three attractors coexist are presented in color. An enlargement of one region of the map for principal parametric resonance reveals a Cantor-like set of fractal boundaries. For some cases, both periodic and chaotic attractors coexist.

Key words: bifurcation theory, chaos, parametric vibrations, quadratic nonlinearity, cubic nonlinearity, fractal basin.

1. Introduction

We consider the response of a single-degree-of-freedom system with quadratic and cubic nonlinearities to a harmonic parametric excitation. The problem is governed by

$$\ddot{u} + 2\varepsilon\mu\dot{u} + \omega_0^2 u + \varepsilon\delta u^2 + \varepsilon^2\alpha u^3 + \varepsilon g u\cos\Omega t = 0, \tag{1}$$

where the dots indicate differentiation with respect to time, ε is a small dimensionless parameter, and μ, ω_0, δ, α, g, and Ω are constants. Equation (1) describes the response of a single-degree-of-freedom mechanical system or a one-mode approximation to the response of an arch, beam, plate, or shell. The quadratic term may be due to curvature or an asymmetric material nonlinearity whereas the cubic term may be due to mid-plane stretching or a symmetric material nonlinearity. The parametric term may be due to a harmonic axial or inplane load or a rotating element. For a comprehensive review of the response of single- and multi-degree-of-freedom systems to parametric excitations, the reader is referred to the textbooks of Bolotin [1], Evan-Iwanowski [2], Nayfeh and Mook [3], and Ibrahim [4].

Neglecting the nonlinear and damping terms and using Floquet theory [1, 3], one can show that equation (1) possesses solutions that decay with time (stable) and solutions that grow with time (unstable). Moreover, one can draw a stability chart in the space of the parameters of the equation that separates the parameter space into regions of stability and instability. For this equation the stability chart is called the Strutt diagram [5] and it separates the $(4\omega_0^2/\Omega^2, 4\varepsilon g/\Omega^2)$ plane into regions of stability and instability. Resonances occur when $4\omega_0^2/\Omega^2 \approx n^2$, where n is an integer. The asymptotic expansions of the transition curves are given in powers of $4\varepsilon g/\Omega^2$.

We note that modeling a system that is subjected to a parametric excitation by linear equations and boundary conditions is unrealistic if the parametric excitation leads to an instability

Nonlinear Dynamics **1**: 1–21, 1990

because it results in unlimited amplitudes. The growth of the response is exponential. Including damping in the analysis usually diminishes the region of instability but sometimes it may change a stable region into an unstable region, especially for the case of combination resonance [3]. The growth of the unstable solutions is exponential and hence unrealistic. Consequently, a more realistic model includes nonlinear terms which act as limiters of the response. Moreover, the linear model may predict a stable parametric response (i.e., decaying response), whereas the actual response may not decay under certain conditions. In this case, the parametric excitation produces a subcritical instability that is only predictable by including nonlinear terms. Furthermore, nonlinearity brings a whole range of phenomena that are not found in linear systems. In single-degree-of-freedom systems governed by equation (1), these phenomena include multiple solutions, jumps, limit cycles, resonances, period-multiplying and cyclic-fold bifurcations, and chaos. In this paper, we demonstrate some of these phenomena by using perturbation methods and digital- and analog-computer simulations.

2. Global Behavior

The system described by equation (1) has many attractors (long-time responses). The number and type of attractors observed depend on the initial conditions and the parameters ε, μ, ω_0, δ, α, g, and Ω. A complete characterization of the dynamics of the system would include the behavior of its long-time solutions (attractors) and their basins of attraction as the system's parameters are varied. To keep the problem within a manageable size, we limit the number of parameters considered. Here, we assume that only one of these parameters can be varied at a time; that is, only co-dimension one bifurcations [6] are considered.

The equilibrium positions of the undamped and unexcited system described by equation (1) can be found by setting the excitation amplitude g, damping coefficient μ, and all time-derivative terms equal to zero. The resulting equation yields the equilibrium positions

$$u = 0\,, \qquad (2\varepsilon\alpha)^{-1}[-\delta \pm (\delta^2 - 4\omega_0^2\alpha)^{1/2}]\,. \tag{2}$$

The number and type of equilibrium positions as well as the shape of the potential depend on the values of α, δ, ω_0, and ε. When $\omega_0 = 1.0$, $\alpha = 4.0$, and $\varepsilon = 0.1$, we have the cases shown in Figure 1. When $\delta = 5.0$ there are two stable equilibrium points (centers) and one unstable equilibrium point (saddle). When $\delta = 4.0$, the radical vanishes and the left center and saddle point merge to form a cusp; when $\delta = 3.0$, the only real root is the origin. Phase-plane plots and potential energy diagrams are shown in Figure 1 for these three cases.

Motions around the stable equilibrium points were determined [7–9] using the method of multiple scales [10, 11], whereas motions encircling all equilibrium points were determined using analog and digital computations. We note that case c, having a double-well potential, exhibits the most interesting behavior. Thus, we concentrate the analog- and digital-computer analysis on this case.

In analyzing systems under forced oscillations, it is useful to determine the effect of changes in the excitation on the behavior of the system. From an engineering point of view, it is critical to identify the excitation parameters that could lead the system into potentially catastrophic responses.

In this section, we present the results of the analysis of qualitative changes (bifurcations)

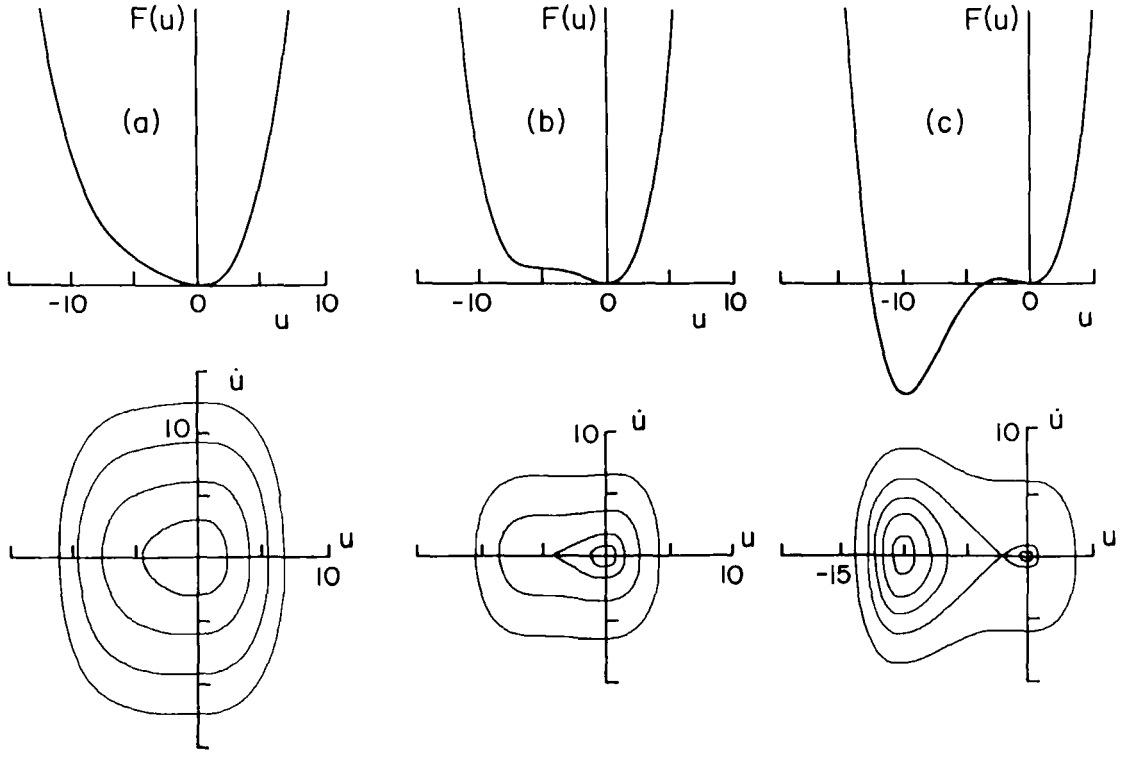

Fig. 1. Potential wells and corresponding phase-plane portraits for three distinct cases: (a) $\delta = 3.0$, (b) $\delta = 4.0$, (c) $\delta = 5.0$, for $\alpha = 5.0$, $\mu = 1.0$, and $\varepsilon = 0.10$. The phase-plane portraits were obtained on the analog computer.

occurring in the long-time solutions (attractors) described by equation (1) as the amplitude g or frequency Ω of the excitation is slowly changed. The results are summarized in what is called a state or bifurcation diagram, which presents transition curves enclosing regions of stability in a two-dimensional parameter space consisting of g and Ω, where it is assumed that only one of them is varied at a time across any transition curve. The results presented in this section were obtained for the parameters $\alpha = 4.0$, $\delta = 5.0$, $\omega_0 = 1.0$, $\varepsilon = 0.1$, and $\mu = 1.0$, corresponding to the case of the double-well potential.

To determine the global bifurcations, we used an analog computer to simulate the system described by equation (1), a signal analyzer to determine the power spectrum (Fast Fourier Transform, FFT) of the response signal, and an oscilloscope to display the phase portraits of the output signals consisting of u and $\dot{u}$. We began the simulation by fixing g and Ω and choosing initial conditions. We waited until a steady state was reached, as indicated by no variations in the displays of the FFT, phase portrait, and Poincaré map. Then, we recorded the values of the excitation parameters g and Ω and plotted the phase portrait, Poincaré map, and FFT of the attractor, which may be a point, a limit cycle, or a chaotic attractor. Fixing the excitation parameters, we slowly varied the initial conditions to locate other attractors if they existed. Then, we gradually changed one of the excitation parameters and observed qualitative changes in the phase portrait, Poincaré map, and FFT to locate the bifurcations.

Near the bifurcation points, a steady-state solution may require many cycles to develop and this can be expensive on a digital computer. For example, to achieve a steady-state solution may require 50,000 cycles (of the excitation) with 100 points per cycle using a 5th- and 6th-order

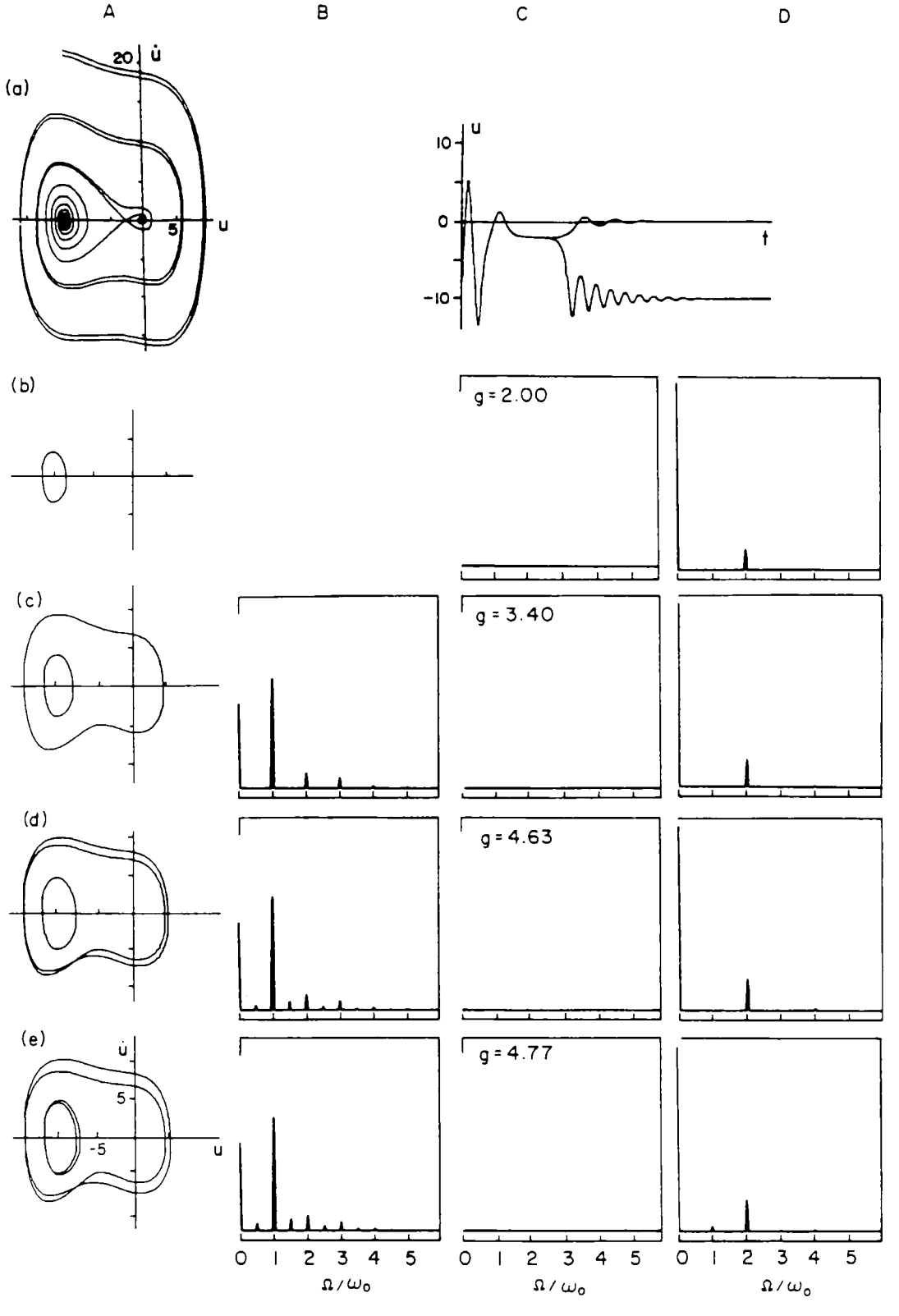
A
B
C
D
(a)
20
u̇
5
u
10
u
0
t
-10
(b)
g = 2.00
(c)
g = 3.40
(d)
g = 4.63
(e)
u̇
5
-5
u
g = 4.77
0 1 2 3 4 5
Ω / ω₀
0 1 2 3 4 5
Ω / ω₀
0 1 2 3 4 5
Ω / ω₀

Figs. 2(a)-(e).

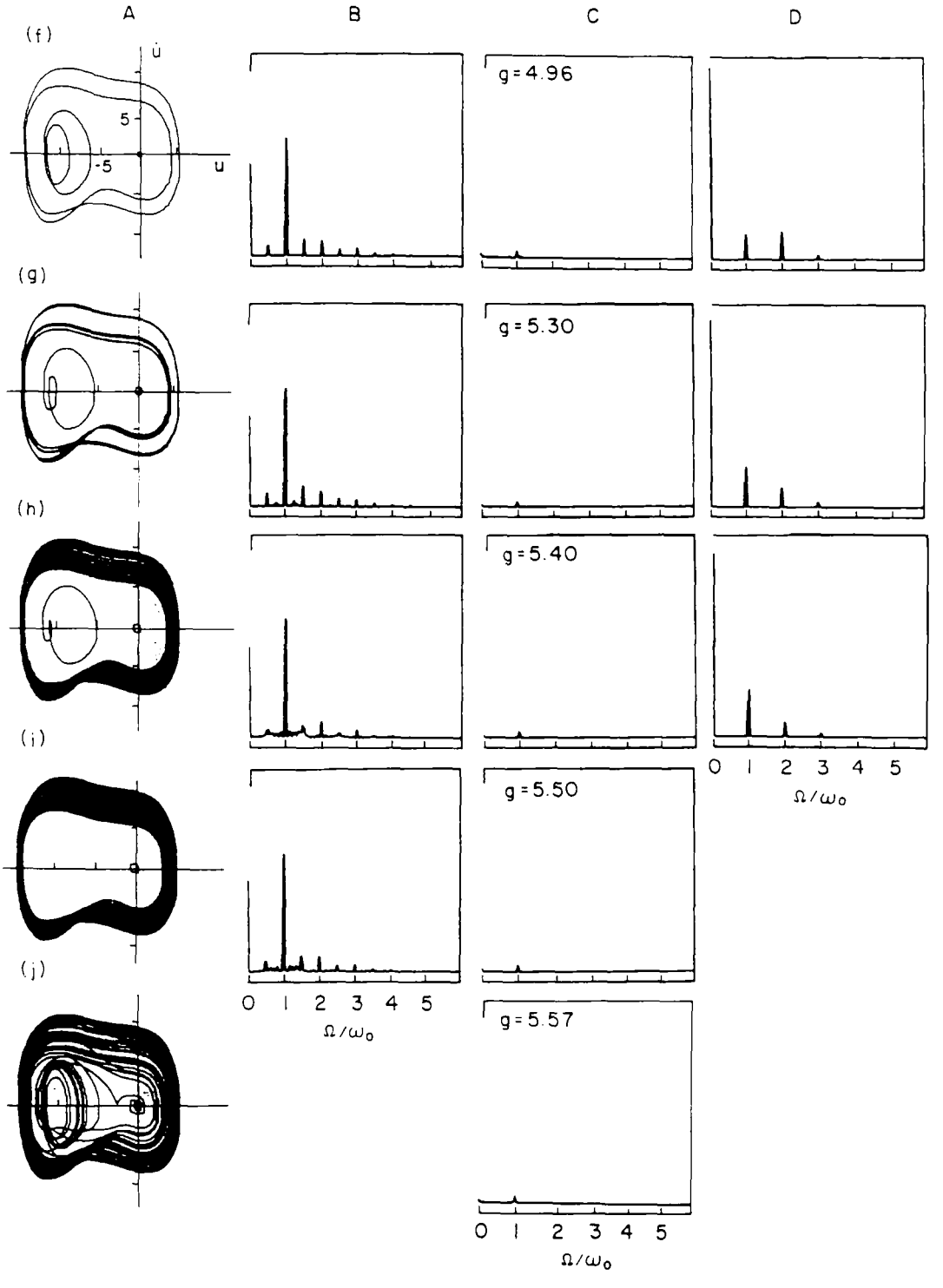

Figs. 2(f)-(j).

Fig. 2. Phase-plane portraits and accompanying power spectra of the response obtained by analog-computer simulation when $\Omega = 2$.

Runge–Kutta–Verner algorithm. However, on the analog computer, these bifurcation points can be easily located because the integration process can be speeded up and only seconds are needed to achieve a steady-state solution when operating in a high speed mode (accomplished by time scaling the computer). Once a steady state has been achieved, any system parameter can be varied continuously, thus slightly disturbing the system from its steady-state response. In this manner, an attractor that has a very small domain of attraction and/or domain of existence may be realized by starting with system parameters that enlarge its domain of attraction and/or existence.

As an example, Figure 2 shows the results obtained by keeping Ω fixed at 2.0 and varying only the amplitude of the excitation. These results show multiple attractors including the simultaneous coexistence of a limit cycle and a chaotic response, the familiar period-doubling bifurcations leading both to chaos and extinction, and windows of $3\times$, $6\times$, $7\times$, and $12\times$ bifurcations within the chaotic regions. In addition, their corresponding frequency spectra are shown in column B for the large-amplitude attractors enclosing the three equilibrium positions, in column C for the small-amplitude attractors encircling the right equilibrium position, and in column D for the nontrivial attractors enclosing the left equilibrium position.

A periodic orbit of a dissipative system of the type described by equation (1) is known to lose stability through two types of bifurcations [6]: period-doubling (flip) or cyclic-fold (saddle-node, tangent, turning-point) bifurcations. For each attractor there is a region of parameter space in which it exists; this region is enclosed by bifurcation curves across which qualitative changes occur in the response of the system; that is, the response of the system changes from one attractor to another. The period-doubling bifurcation is often the beginning of a full sequence of period-doubling bifurcations, leading to a chaotic attractor. On the other hand, the cyclic-fold bifurcation is associated with a jump to another attractor which exists in the same region of parameter space. Similarly, a point attractor in this system may lose its stability, resulting in a jump to another point attractor or a periodic attractor.

Figure 3 shows a small region of parameter space $g - \Omega$ (scaling Ω with respect to ω_0 to make it nondimensional) where four attractors coexist: three periodic attractors and one point attractor can be obtained by choosing appropriate initial conditions. The attractors are shown in the insets (a)–(d) at a typical point. Attractor (a) exists in region A below the curve 1–2, which is a

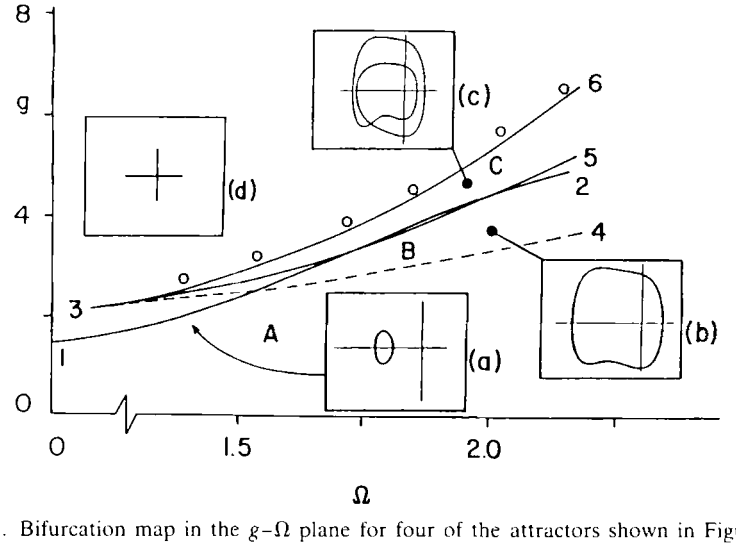

Fig. 3. Bifurcation map in the g–Ω plane for four of the attractors shown in Figure 2.

period-doubling boundary. As a parameter is changed by crossing the curve, a period-doubling bifurcation takes place. In a very narrow region near curve 1–2 another bifurcation (a cyclic-fold-not shown) takes place inducing a jump to a larger attractor. Attractor (b) exists in area B formed by a wedge that comes from the right enclosed by curves 3–4 and 3–5, corresponding to cyclic-fold (saddle-node) and period-doubling bifurcations. If a parameter is varied across 3–4 by moving to the region below it, the attractor becomes unstable and a jump to a point attractor at the origin is observed; the origin, attractor (d), is stable throughout the figure. On the other hand, a variation across 3–5 induces a period-doubling bifurcation that causes attractor (b) to transform into attractor (c) and vice versa. Attractor (c) is stable between 3–5 and 3–6. When crossing 3–6, attractor (c) undergoes a sequence of period-doubling bifurcations leading to chaos. The circles mark the points where chaotic behavior was observed during simulation.

The global structure of the state or bifurcation diagram can be characterized as wedges or tongues in the parameter space; these wedges show the range of parameters which, given proper initial conditions (depending on the basin), leads to the attractor. The boundaries of the wedges are coded to indicate the types of instabilities to be observed when a parameter value is slowly varied across the curve. The bifurcation diagram provides useful information regarding the instabilities of the system and the behaviors that are most likely to occur after the instability.

Figures 4 and 5 summarize the results of extensive analog simulations of equation (1) for a broad portion of the parameter space $g - \Omega$. These figures represent the qualitative description of the behavior of the system to local changes in the amplitude or frequency of excitation. The

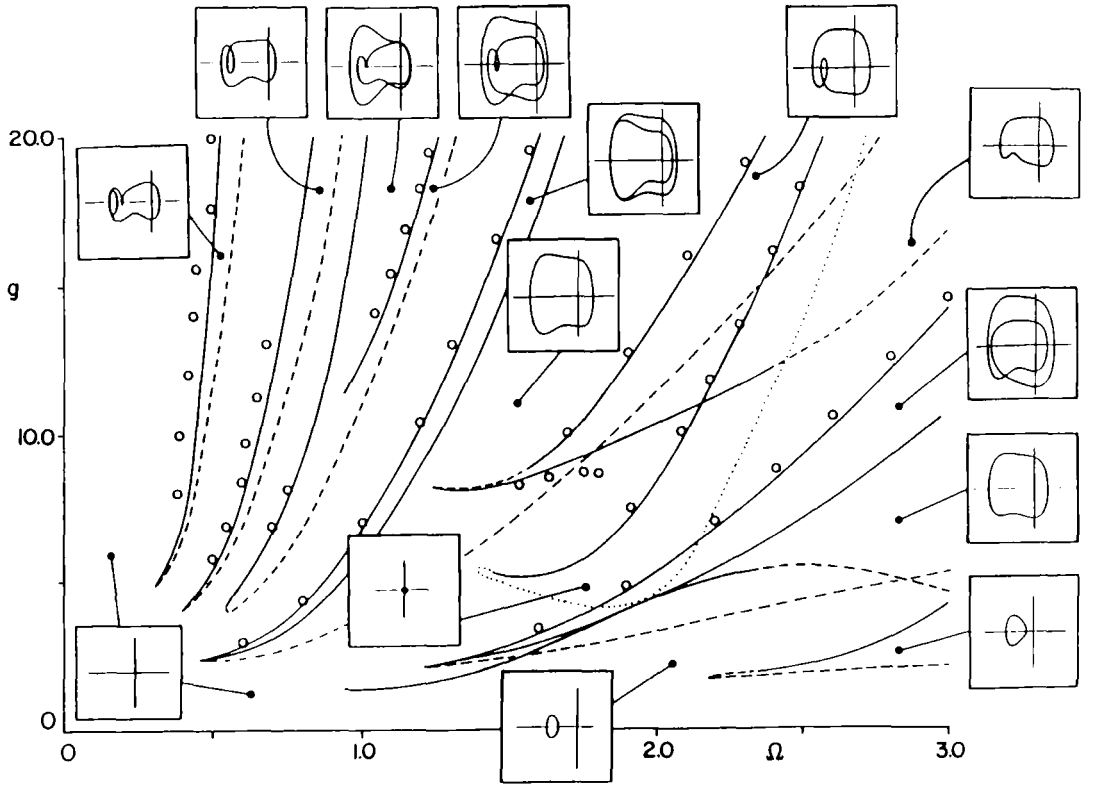

Fig. 4. Bifurcation map for a broad portion of the g–Ω plane for $\alpha = 4.0$, $\delta = 5.0$, $\mu = 1.0$, and $\varepsilon = 0.10$.

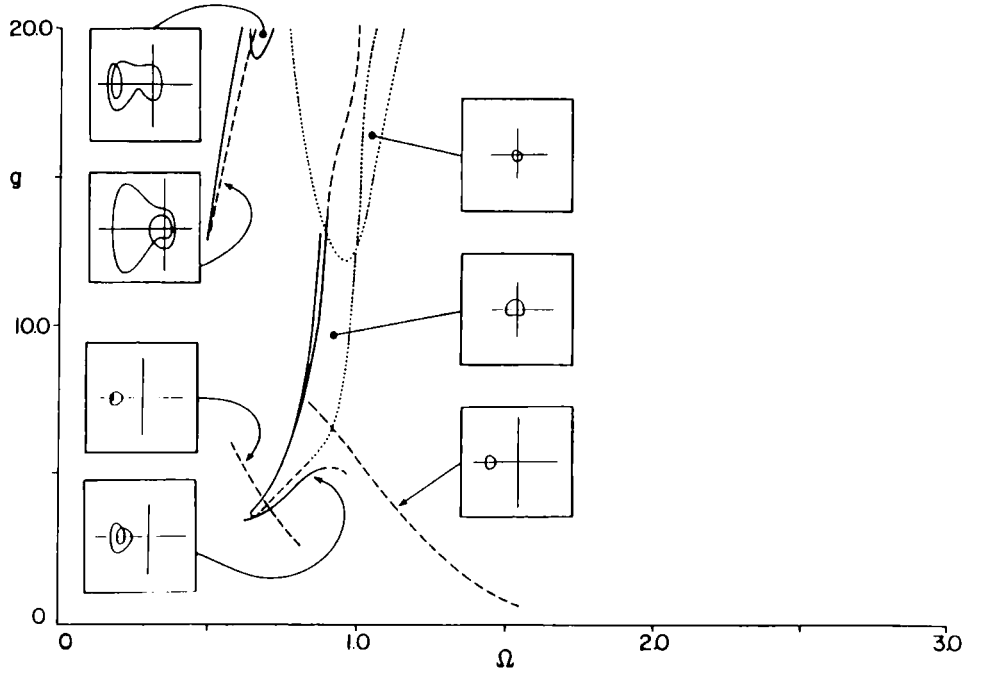

Fig. 5. Additional attractors and their bifurcation boundaries.

diagram is not complete in some regions of the parameter space; in particular, in the super-harmonic region, the coexistence of attractors with complicated and entangled basins makes the mapping task very cumbersome.

Figure 4 shows fourteen typical attractors which undergo bifurcations similar to those shown in Figure 3. The lines are coded as follows: solid lines represent period-doubling bifurcations, dashed lines show cyclic-fold instabilities, and dotted lines show transcritical bifurcations of the trivial attractor. Figure 5 is actually part of Figure 4 and is shown separately for clarity. Most attractors exist in a wedge-shaped stable region mentioned before and enclosed by bifurcation curves. As shown in Figure 4, the wedge typically has a period-doubling bifurcation on its upper left portion and a cyclic-fold bifurcation on its lower right portion. As in Figure 3, the circles represent the locations where chaotic behavior was observed. The areas where the wedges intersect represent coexistence (multistability) of attractors (solutions). In these cases, there is the possibility that once an attractor becomes unstable the system would jump to another attractor in the region.

3. Fundamental Parametric Resonance

Fundamental parametric resonance occurs when the excitation frequency is nearly equal to the linear natural frequency of the system (i.e., $\Omega \approx \omega_0$). It is not, however, the most common parametric resonance. It requires a larger forcing amplitude for its activation. A detailed analysis of this system, including a perturbation analysis and extensive simulation on both the digital and analog computers can be found in Zavodney and Nayfeh [8].

For small oscillations about the origin, an approximate solution of equation (1) is given by

$$u = a\cos(\omega_0 t + \beta) + \varepsilon\{(\delta a^2/6\omega_0^2)\cos(2\omega_0 t + 2\beta) + [ga/2\Omega(\Omega + 2\omega_0)]\cos[(\Omega + \omega_0)t + \beta] + [ga/2\Omega(\Omega - 2\omega_0)]\cos[(\Omega - \omega_0)t - \beta] - \delta a^2/2\omega_0^2\} + \cdots, \tag{3}$$

$$\dot{a} = -\varepsilon\mu a + (5\varepsilon^2\delta g a^2/24\omega_0^3)\sin\gamma + (\varepsilon^2 g^2 a/8\omega_0^2)\sin 2\gamma, \tag{4}$$

$$a\dot{\gamma} = \varepsilon^2\left[\left(\frac{\mu_2}{2\omega_0} + \frac{g^2}{12\omega_0^3}\right)a - \alpha_c a^3\right] + \frac{5\varepsilon^2\delta g a^2}{8\omega_0^3}\cos\gamma + \frac{\varepsilon^2 g^2 a}{8\omega_0^3}\cos 2\gamma + \varepsilon^2\sigma a, \tag{5}$$

where

$$\varepsilon^2\sigma = \Omega - \omega_0, \qquad \gamma = \varepsilon^2\sigma t - \beta \tag{6}$$

and

$$\alpha_c = (3\alpha/8\omega_0) - (5\delta^2/12\omega_0^3). \tag{7}$$

Equations (4)–(6) have five possible fixed-point solutions: however, at most only three are stable. For the case of the single-well potential in Figure 1a the effect of varying the amplitude of a perfectly tuned excitation force is shown in Figure 6. The results show that there are four bifurcation values of the excitation amplitude; they divide the excitation amplitude axis into five intervals. Hence, the nonlinearity is seen to do four things: (a) it causes the linear boundary

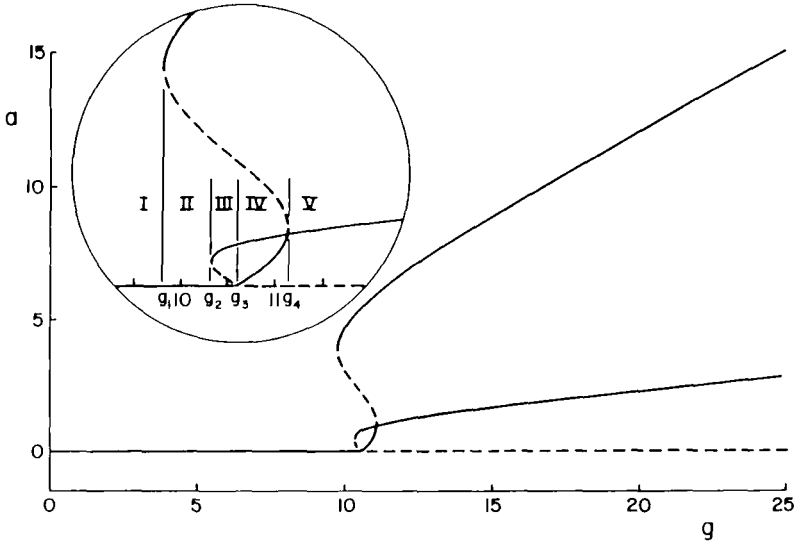

Fig. 6. Variation of the steady-state response amplitude a with the excitation amplitude g showing stable (–) and unstable (---) regions for $\sigma = 0.0$, $\alpha = 4.0$, $\delta = 3.0$, $\mu = 1.0$, $\Omega = 1.0$, and $\varepsilon = 0.10$.

(which would be a straight vertical line at $g = 11.1394$) to bend over to the right, yielding finite-amplitude responses, (b) it causes the boundary curve to bifurcate into two boundary curves, (c) it causes the amplitude-response curve to fold over itself resulting in multiple solutions in certain intervals, and (d) because of the folding, it causes a subcritical instability. The significance of these effects is to limit the infinite response amplitudes predicted by linear theory to finite values and admit finite-amplitude solutions for values of the excitation amplitude that are below the critical value determined from a linear analysis. The accuracy of the perturbation solution given by equations (3)–(7) was verified by numerically integrating the original differential equation (1). A comparison of the analytically predicted responses and the numerically obtained responses is shown in Figures 7 and 8. The frequency- response curve, which could be either

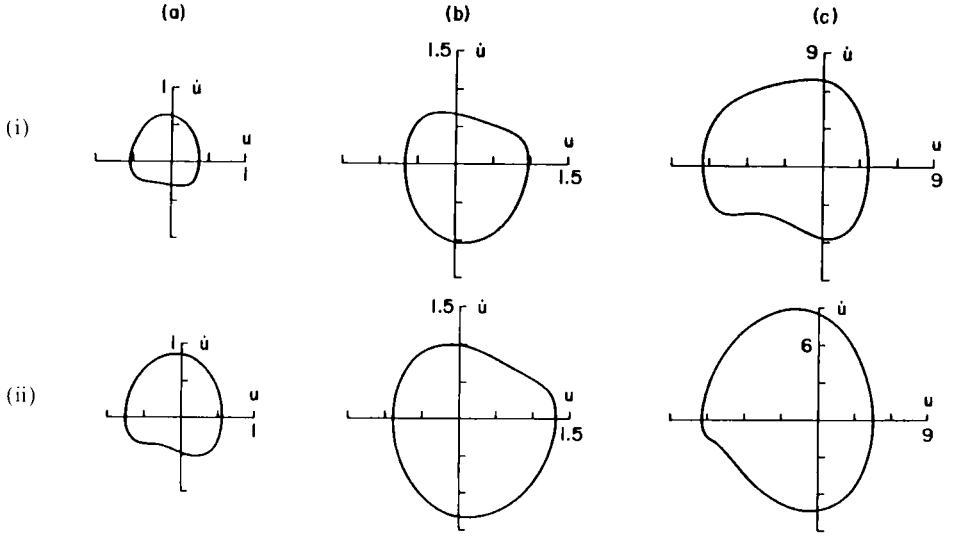

Fig. 7. Phase-plane portraits of the three steady-state solutions obtained by (i) numerical integration and (ii) as predicted by the perturbation solution for $\sigma = 0.0$, $\alpha = 4.0$, $\delta = 3.0$, $\mu = 1.0$, $g = 11.0$, $\Omega = 1.0$, and $\varepsilon = 0.10$.

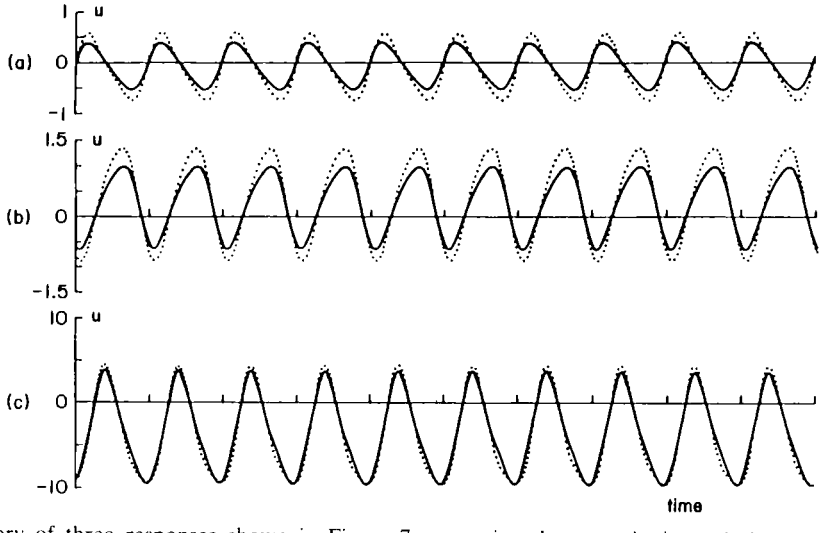

Fig. 8. Time history of three responses shown in Figure 7 comparing the perturbation solution (· · ·) with numerical integration (—).

hardening (by bending over to the right) or softening, is shown in Figure 9. This figure shows five solutions for certain values of detuning. Again we see that the effect of the nonlinearity is to introduce multiple solutions and limit the response amplitudes to finite values. The region on the frequency axis where the trivial solution is unstable corresponds to the instability region predicted by linear theory. As shown here, the nonlinearity extends the region for parametric instability predicted by linear theory to the right slightly and to the left significantly. From Figure 6, we see only a slight extension of the region of parametric instability to the left for the perfectly tuned case.

For the case of the double-well potential shown in Figure 1c, oscillations about the left well are governed by

$$\ddot{x} + 0.2\dot{x} + 3x + 0.7x^2 + 0.04x^3 + 0.1gx\cos\Omega t = g\cos\Omega t \tag{8}$$

This equation was obtained from equation (1) by the linear transformation $x = u + 10$, which shifts the coordinate system so that the left equilibrium position is located at the origin. We note that the linear natural frequency of the system for oscillations about the left equilibrium position is $\sqrt{3}$. In general, the linear natural frequency in a well depends upon the system parameters. Furthermore, it follows from equation (8) that these oscillations are now subject to combined parametric and external (additive) excitations. Consequently, nontrivial attactors will occur in the left well for all values of excitation below that corresponding to the collision of these attractors with the unstable limit cycle, including those for which no steady-state parametric responses exist about the origin in the right well. However, because the input is a combination of external and parametric excitations, it is possible that the interaction of the two excitations can either quench or accentuate the resonance [7]. Furthermore, when the amplitude of vibration becomes large enough, the trajectories will escape the left well.

When the amplitude of excitation is increased to $g = 4.50$, large-amplitude oscillations about all three equilibrium positions are possible. Because three attractors coexist, the initial conditions determine the steady-state response, as shown in Figure 10. Using a digital computer, we repeated

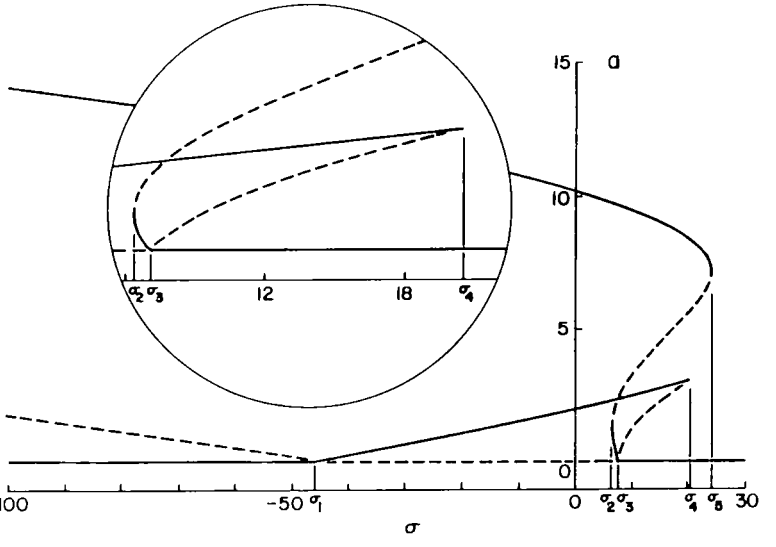

Fig. 9. Variation of the steady-state amplitude a with the frequency detuning σ showing stable (—) and unstable (· · ·) regions for $\alpha = 4.0$, $\delta = 3.0$, $\mu = 1.0$, $g = 15.0$, $\Omega = 1.0$, and $\varepsilon = 0.10$.

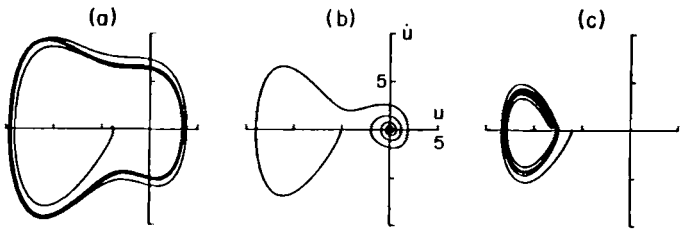

Fig. 10. Phase-plane portraits and trajectories leading to the three attractors for $\sigma = 0.0$, $\alpha = 4.0$, $\delta = 5.0$, $\mu = 1.0$, $g = 5.0$, $\Omega = 1.0$, and $\varepsilon = 0.10$. The initial conditions used were $\dot{u}(0) = 0$ and (a) $u(0) = -4.0$, (b) $u(0) = -5.0$, (c) $u(0) = -6.0$.

this procedure over the domain $-20 \leq u \leq 10$ and $-20 \leq \dot{u} \leq 20$ using a step size of 0.10 and obtained a map that contains 120,699 points corresponding to sets of initial conditions (IC's) and consequently, the same number of numerical integrations of equation (1) of sufficient duration to insure a steady state. By color coding the attractors, one can easily see the domains of attraction, as shown in Figure 11. Some have even introduced shades of the base color to indicate a third dimension; for example, by dividing the time required to reach steady state into five groupings, the IC's that take the response to the red attractor could be subdivided into five shades of red, each darker shade corresponding to a longer time required to achieve steady state. From this basin map, we can conclude that it would be very difficult to predict which steady-state solution would constitute the response; however, we note that the trivial solution has the fewest number of points, so statistically, it would be the least likely response. One could count the number of points that belong to each attractor and give a probability based on these numbers.

As the amplitude of excitation is increased above 4.50, many bifurcations take place, as shown in the bifurcation map in Figure 4. There are several regions of chaos, which always appear on the left side of and above the bifurcation boundaries. One of these chaotic attractors, when $g = 22.0$, is shown in Figure 12a. A Poincaré map for this attractor is shown in Figure 12b at the instant the excitation reached its maximum value (zero phase angle). The Poincaré maps for other selected values of the phase angle are shown in Figure 13.

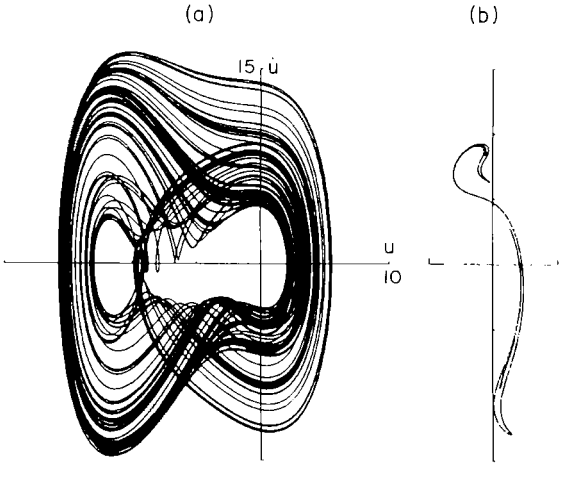

Fig. 12. Phase-plane portrait (a) and Poincaré map (b) of the system obtained by numerical integration of equation (1) showing a chaotic response for $\sigma = 0.0$, $\alpha = 4.0$, $\delta = 5.0$, $\mu = 1.0$, $g = 22.0$, $\Omega = 1.0$, and $\varepsilon = 0.10$.

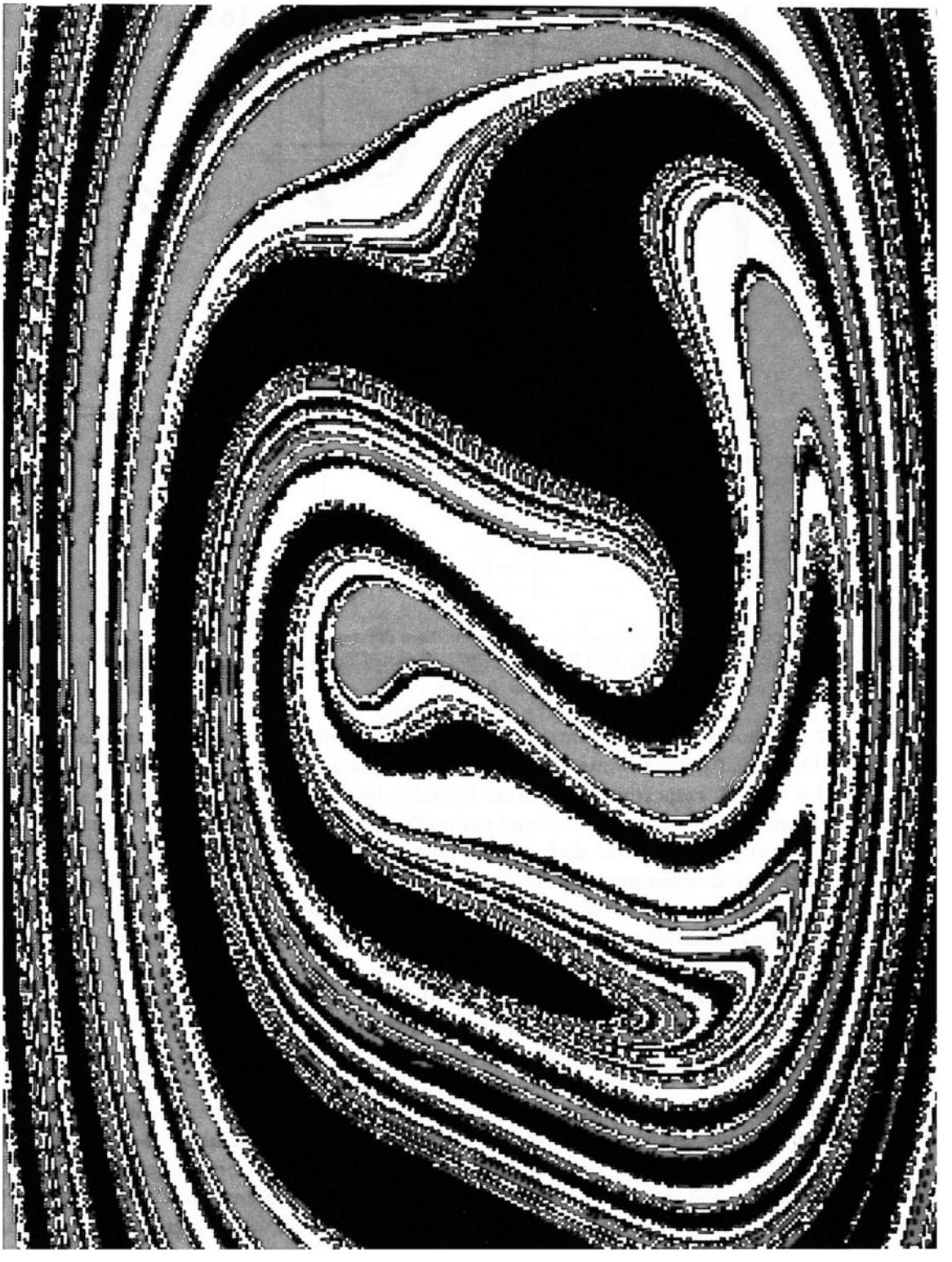

Fig. 11. Fractal basin boundaries separating the domains of attraction for the three attractors shown in Figure 10; black denotes the large outer attractor, red denotes the attractor in the left well centered over the focus at $u = -10$, and white denotes the trivial attractor at the origin. The variable ranges are $-20 \leq u \leq 10$ and $-20 \leq \dot{u} \leq 20$ using a step size of 0.10.

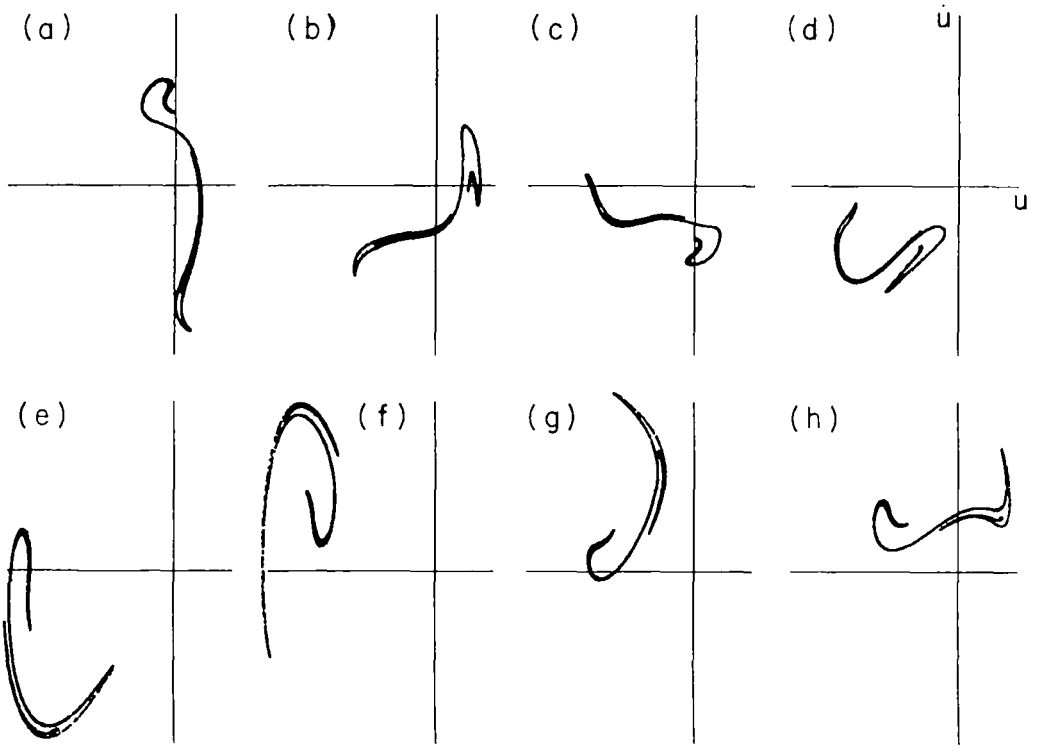

Fig. 13. Poincaré maps of the chaotic attractor shown in Figure 12 at different phase angles of the excitation; (a) $\phi = 0°$, (b) $\phi = 45°$, (c) $\phi = 90°$, (d) $\phi = 135°$, (e) $\phi = 180°$, (f) $\phi = 225°$, (g) $\phi = 270°$, and (h) $\phi = 315°$.

Although not shown on the bifurcation map, we found solutions that had period six and, after a period doubling, had period twelve motion. These periodic attractors appeared for values of $g = 20.57$ and $g = 20.63$, respectively, and were bounded by chaotic attractors on both sides. We found period seven attractors for $g = 22.6$ and period three attractors for $g = 22.7$. These periodic attractors were bounded by chaotic attractors on both sides, but appeared to jump between the period three and period seven motions. To realize them required an extensive amount of time. These attractors did not appear to follow the typical period-multiplying and demultiplying bifurcations leading to and from chaos. In addition to the exotic attractors found on the analog computer, we found period five and period seven motions on the digital computer.

When nonlinearity is included in the damped Mathieu equation, the damping continues to play a minor role in the case of fundamental parametric resonance. For selected values of negative detuning, the variation of the response amplitude with the damping coefficient is shown in Figure 14. This behavior has two distinctive features: (a) the curves are initially relatively flat, which implies that increases in the damping coefficient do not significantly affect the resonance, and (b) a critical value of damping, always exceeding the value determined from a linear analysis, must be exceeded before the resonance can be attenuated for all possible initial or disturbed states. For all of the large-amplitude and most of the small-amplitude cases, the suppression is a jump behavior caused by a cyclic-fold bifurcation. This behavior is in sharp contrast with the gradual attenuation in the response amplitude caused by a gradual increase in the damping coefficient that occurs in externally excited systems. We refer the reader to Zavodney and Shihada [12] for a discussion of the role of damping in parametrically excited systems.

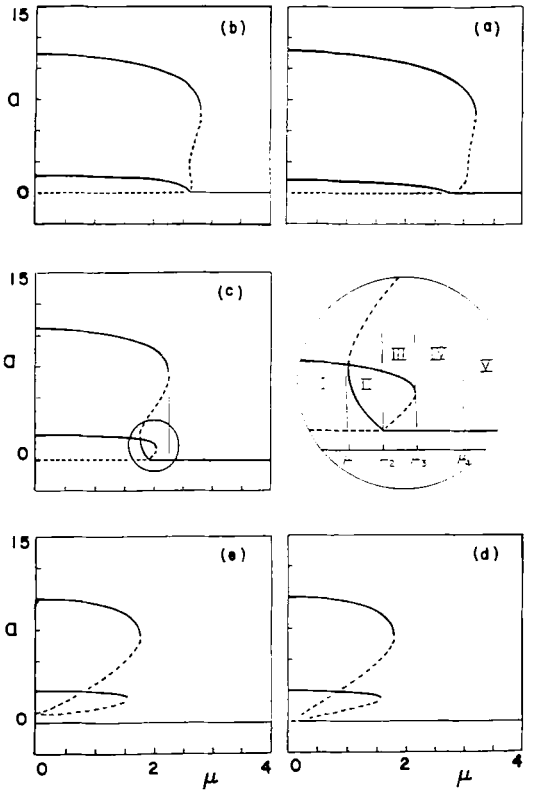

Fig. 14. Variation of the amplitude with the damping coefficient μ for selected frequencies of excitation; stable (—) and unstable (· · ·) responses for $\alpha = 4.0$, $\delta = 3.0$, $g = 15.0$, $\Omega = 1.0$, and $\varepsilon = 0.10$: (a) $\sigma = -15.0$, (b) $\sigma = -12.0$, (c) $\sigma = 0.0$, (d) $\sigma = 9.0$, (e) $\sigma = 12.0$.

4. Principal Parametric Resonance

A principal parametric resonance occurs when the excitation frequency is nearly twice the linear natural frequency of the system (i.e., $\Omega \approx 2\omega_0$). It does not require as large an excitation amplitude for its activation as the second-order fundamental parametric resonance because it is a first-order resonance. A detailed analysis of this system, including a perturbation analysis and extensive simulation on both the digital and analog computers can be found in Zavodney *et al.* [9]. Szemplinska-Stupnicka *et al.* [13] treated the case of symmetric two-well potentials. They used approximate solutions to predict the stability of periodic solutions in a well as precursors to chaos. Nayfeh and Sanchez [14, 15] used a combination of second-order perturbation solutions and Floquet theory to determine symmetry-breaking, flip, and cyclic-fold bifurcations as precursors to chaos and unbounded motions.

For small oscillations in the right well centered about the origin (one of the implicit assumptions underlying the perturbation solution that restricts motions to small but finite oscillations), the perturbation solution is given by:

$$u = a\cos\left(\frac{1}{2}\,\Omega t - \frac{1}{2}\,\gamma\right) + \varepsilon\left\{\frac{1}{6}\,\delta a^2\cos(\Omega t - \gamma) + \frac{ga}{2\Omega(\Omega + 2\omega_0)}\cos\left[\frac{3}{2}\,\Omega t - \frac{1}{2}\,\gamma\right] - \frac{1}{2}\,\delta a^2\right\} + \cdots, \tag{9}$$

$$\dot{a} = -\varepsilon\mu a - \frac{\varepsilon g}{4\omega_0}\left(1 - \frac{\varepsilon\sigma}{2\omega_0}\right)a \sin\gamma, \tag{10}$$

$$a\dot{\beta} = \varepsilon^2\left[\left(\frac{3g^2}{64\omega_0^3} - \frac{\mu^2}{2\omega_0}\right)a + \alpha_e a^3\right] + \frac{\varepsilon g}{4\omega_0}\left(1 - \frac{\varepsilon\sigma}{2\omega_0}\right)a\cos\gamma, \tag{11}$$

$$\varepsilon\sigma = \Omega - 2\omega_0 \qquad \text{and} \qquad \gamma = \varepsilon\sigma t - 2\beta. \tag{12}$$

The frequency-response equation in this case is given by

$$\varepsilon\alpha_e a^2 = \frac{1}{2}\sigma - \frac{3\varepsilon g^2}{64\omega_0^3} + \frac{\varepsilon\mu^2}{2\omega_0} \pm \left[\frac{g^2}{16\omega_0^2}\left(1 - \frac{\varepsilon\sigma}{2\omega_0}\right)^2 - \mu^2\right]^{1/2}. \tag{13}$$

The variation of the steady-state response amplitude with the amplitude of excitation is shown in Figure 15. Both principal and fundamental parametric resonances exhibit the effect of the nonlinearity on the system response; it limits the infinite responses and causes a folding of the response curve in the direction of the nonlinearity; that is, a folding to the left for a negative detuning and a softening-type nonlinearity and a folding to the right for a positive detuning and a hardening-type nonlinearity. As in the case of fundamental parametric resonance, the overhang causes a subcritical instability. The frequency-response curve is shown in Figure 16 and reveals a softening behavior because it is bent to the left. This behavior is similar to that of the frequency-response curve of the fundamental parametric resonance, which is also bent to the left. This behavior may seem surprising because the coefficients of both the quadratic and cubic nonlinearities are positive. As born out by the perturbation analysis, the effective nonlinearity α_e, which is determined by equation (7), turns out to be negative for the parameters used. We note from equation (7) that the effect of the quadratic nonlinearity is always softening regardless of the sign of δ, whereas the effect of the cubic nonlinearity depends upon the sign of α. So, it is possible to have an effective nonlinearity that is zero for appropriate choices of α and δ. It turns out that the perturbation solution breaks down in this region, hence we need a higher-order perturbation theory for the regions where the effective nonlinearity tends toward zero. Away from this region the perturbation solution gives good results. A phase portrait and the long-time history predicted by the perturbation solution are compared with the results of numerical integration of equation (1) for one of these cases in Figure 17.

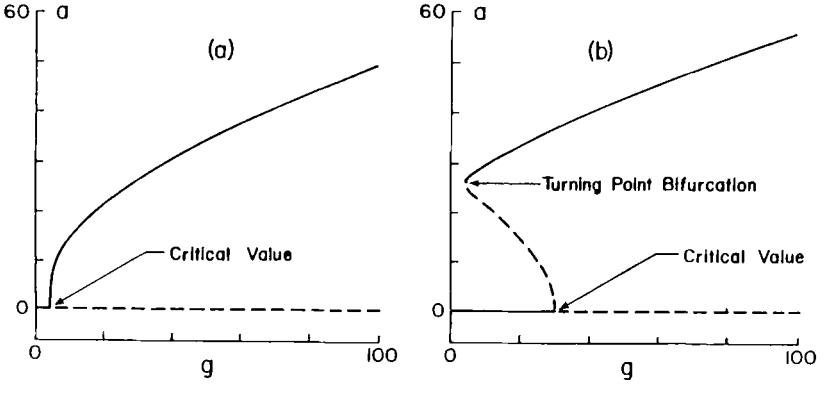

Fig. 15. Variation of the steady-state response amplitude a with the excitation amplitude g showing stable (—) and unstable (· · ·) regions for $\alpha = 4.0$, $\delta = 3.0$, $\mu = 1.0$, $\Omega = 2.0$, and $\varepsilon = 0.005$: (a) $\sigma = 0.0$, and (b) $\sigma = -15.0$.

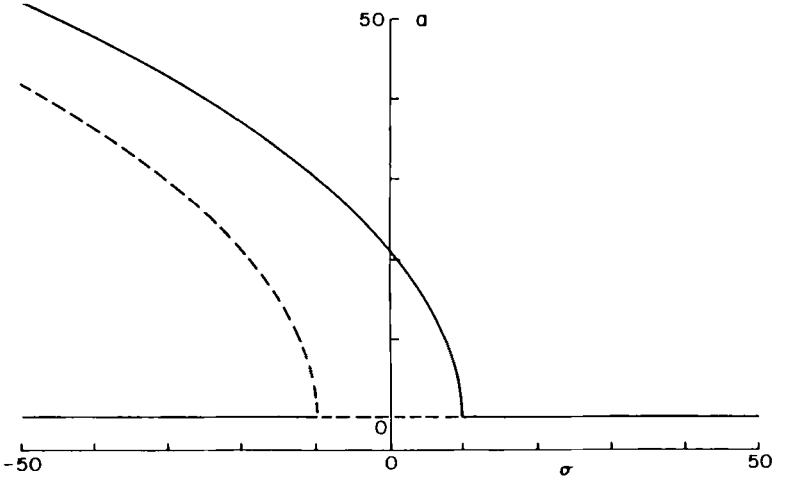

Fig. 16. Variation of the steady-state response amplitude a with the excitation frequency detuning σ showing stable (—) and unstable (---) regions for $\alpha = 4.0$, $\delta = 3.0$, $\mu = 1.0$, $g = 20.0$, $\Omega = 2.0$, and $\varepsilon = 0.005$.

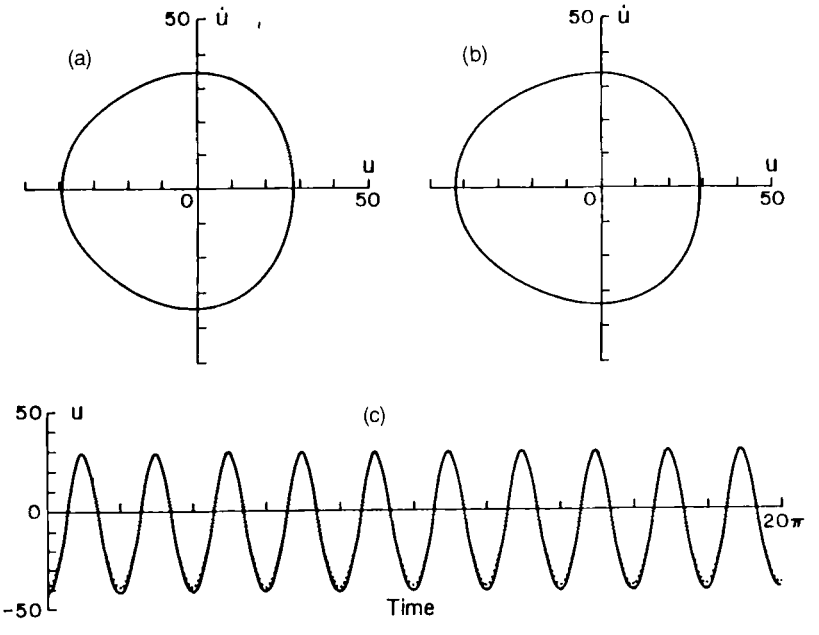

Fig. 17. Phase-plane portraits of the steady-state nontrivial response comparing the (a) perturbation solution with (b) numerical integration of the original equation, and inset (c) shows the time traces of the perturbation solution (· · ·) and numerical simulation (—) superposed for $\alpha = 4.0$, $\delta = 3.0$, $\mu = 1.0$, $g = 20.0$, $\Omega = 2.0$, and $\varepsilon = 0.005$.

As in the case of fundamental parametric resonance, the perturbation solutions obtained are valid for small-amplitude motions about an equilibrium position. When these trajectories become unstable, the response will jump to another attractor. In the case of the double well, there is an attractor in the left well that results from combined external and parametric excitations, as happened in the case of fundamental parametric resonance. As the excitation amplitude is increased to $g = 3.40$, a large-amplitude attractor appears and encircles all three equilibrium positions, as shown in Figure 2. Both attractors (large and in left well) experience period-doubling bifurcations as g increases; the large-amplitude attractor eventually becomes chaotic while the

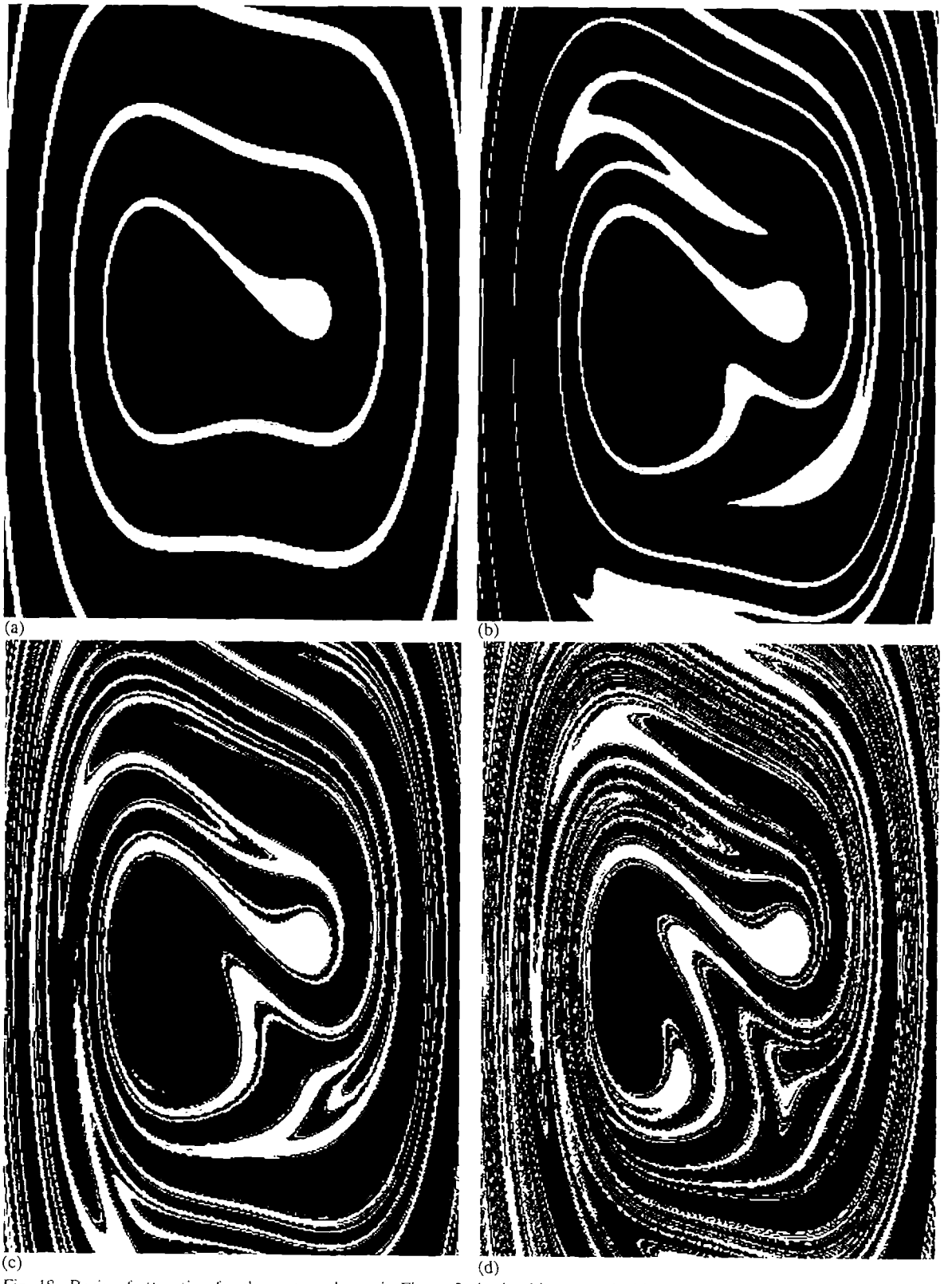

Fig. 18. Basin of attraction for the system shown in Figure 2 obtained by numerical integration for $\Omega = 2$ for the excitation levels (a) $g = 0.0$, (b) $g = 1.5$, (c) $g = 2.0$, and (d) $g = 3.0$. Insets (c) and (d) reveal a fractal boundary. The variable ranges are identical to those in Figure 11.

attractor in the left well never becomes chaotic because of its collision with the unstable limit cycle – it simply loses its stability leaving only the large-amplitude attractor and a point attractor at the origin. As the amplitude g of excitation increases further, the system bifurcates many times; sometimes the trajectories become chaotic and sometimes a chaotic attractor coexists with a periodic attractor. Sometimes one of the attractors will eventually become unstable while the other attractors are unaffected. The behaviors are summarized in the bifurcation diagram in Figure 4.

When the excitation level is increased to $g = 1.5$ starting from $g = 0$, the fixed point at the left equilibrium position bifurcates into a limit cycle. The basins of attraction of this limit cycle and the trivial response at the origin are shown in Figure 18b. We note that the outbound separatrices deform but continue to be smooth. As g is increased to 2.0, the basin boundaries appear to be fractal, as shown in Figure 18c. As g is increased to 3.0, the boundaries become more complicated, as shown in Figure 18d.

Figure 2c shows that when $g = 3.4$, there are three possible responses: a trivial response at the origin because g is below the critical excitation level for the activation of the parametric resonance, a small-amplitude response at the forcing frequency in the left well, and a new large-amplitude attractor that encircles all three equilibrium positions. The unforced response shown in part (a) of Figure 2 shows the two inbound separatrices approaching the saddle point whereupon they branch and spiral into the two attracting foci. These inbound separatrices divide the domain of attraction into two distinct regions: a large region leading to the left attractor and a small region leading to the origin. This behavior was also observed in the digital-computer simulation, as shown in Figure 18a. The displacement of the separatrix that approaches the saddle point from below is plotted as a function of time until it reaches the saddle point; then both outbound separatrices are shown splitting from the equilibrium position and freely oscillating to their foci. When $g = 4.20$, three attractors coexist: the fixed point at the origin, a limit cycle encircling the left equilibrium position, and a large attractor encircling the three equilibrium positions. The basin of attraction for this new attractor is shown in red color in Figure 19a. The basins of attraction appear to be fractal. A small region near the center was enlarged ten times and is shown in Figure 19b. It reveals a Cantor-like set.

5. Summary

In this paper, we have summarized the behavior of a nonlinear dynamical system having quadratic and cubic stiffness terms subject to a harmonic parametric excitation. We have considered a broad frequency range in general and the more common principal and fundamental parametric resonances in particular. Although they have distinct behaviors, they also share some. The nonlinearity is seen to basically limit the exponential growth predicted by linear models even when damping is present. The effects of the quadratic nonlinearity are to contribute to the nonlinear frequency shift, generate the second harmonic, and generate the drift term in the response. The effect of the cubic term is less pronounced because its effects are to contribute to the nonlinear frequency shift and generate the third harmonic observed in the spectra of the responses.

The second-order perturbation expansions give quite good results – both qualitatively and quantitatively for small but finite-amplitude responses about an equilibrium position as long as the first-order nonlinear shift (i.e., $\varepsilon^2\alpha_e a^2$) to the frequency is not near zero. However, when the effective nonlinearity vanishes due to appropriate choices of the coefficients α and δ of the cubic and quadratic nonlinearities, so does the limiting effect of the nonlinearity. Hence, to second

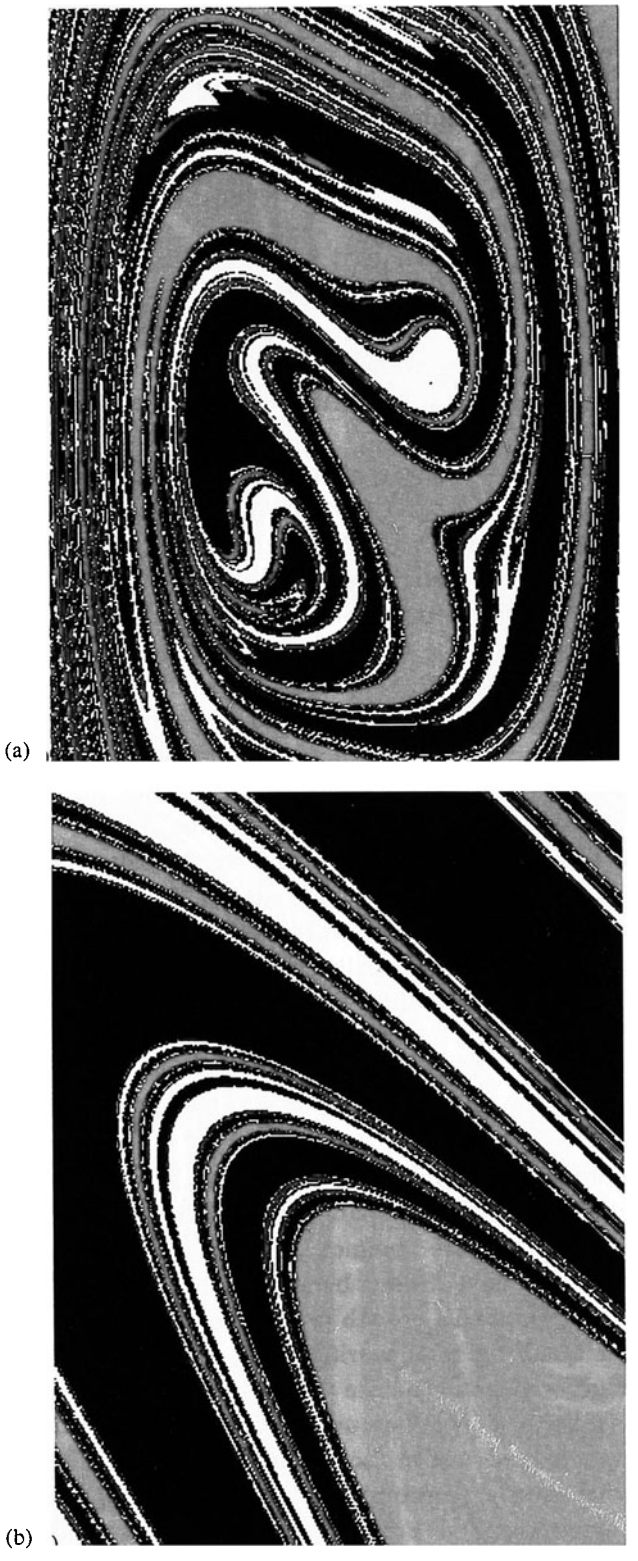

Fig. 19. Basin of attraction for the system shown in Figure 12 for $g = 4.2$. The red region denotes the new large amplitude attractor; (a) variable ranges identical to those in Figure 11, (b) enlarged portion near the center for the variable ranges $-7.2 \leq u \leq -4.2$ and $-2.0 \leq \dot{u} \leq 2.0$.

order, the response is very large, and one needs to carry out the expansion to a higher order.

With sufficiently large excitation levels, many solutions were observed and charted, and their domains of existence were determined. Period-doubling and cyclic-fold bifurcation boundaries were generated using analog-computer simulations. Solutions characterized by period T, 2T, 3T, 4T, 5T, 6T, 7T, 8T, 12T, and 16T were observed in the simulations. Chaotic responses were also observed. For two points in the bifurcation map (one corresponding to a fundamental parametric resonance at $\Omega = 1$ and one corresponding to a principal parametric resonance at $\Omega = 2$) where three attractors coexist, the basin maps showing the domains of attraction were plotted. For the case of principal parametric resonance, three transitionary stages were plotted, showing the development of a fractal boundary from a smooth boundary.

In some cases increasing a control parameter, such as the level of excitation g, causes an attractor to lose stability and go to another attractor but decreasing g to its previous value does not always recover the original attractor due to the coexistence of attractors. Although this is a single-degree-of-freedom system, it displays rich and complicated dynamics and has many coexisting attractors. In some cases, periodic attractors coexist with chaotic attractors.

Acknowledgements

This work was supported by the Army Research Office under Grant No. DAAL03-89-K-0180 and the Office of Naval Research under Contract No. N00014-83-K-0184, NR 4322753. We thank Mr. Tariq Nayfeh for his assistance with some of the analog-computer simulations and the fractal basins and B. Balachandran for his comments on the manuscript.

References

1. Bolotin, V. V., *The Dynamic Stability of Elastic Systems*, Holden-Day, 1964.
2. Evan-Iwanowski, R. M., *Resonance Oscillations in Mechanical Systems*, Elsevier, 1976.
3. Nayfeh, A. H. and Mook, D. T., *Nonlinear Oscillations*, Wiley-Interscience, 1979.
4. Ibrahim, R. A., *Parametric Random Vibration*, Wiley-Interscience, 1985.
5. Strutt, M. J. O., 'On the maintenance of vibrations by forces of double frequency and on the propagation of waves through a medium endowed with a periodic structure', *Phil. Mag.* **24**, 1987, 145–159.
6. Guckenheimer, J. and Holmes, P. J., *Non-linear Oscillations, Dynamical Systems and Bifurcations of Vector Fields*, Springer Verlag, Berlin, 1983.
7. Nayfeh, A. H., 'Interaction of fundamental parametric resonances with subharmonic resonances of order one-half', *J. Sound Vib.* **96**, 1984, 333–340.
8. Zavodney, L. D. and Nayfeh, A. H., 'The response of a single-degree-of-freedom system with quadtratic and cubic nonlinearities to a fundamental parametric resonance', *J. Sound Vib.* **120**, 1988, 63–93.
9. Zavodney, L. D., Nayfeh, A. H., and Sanchez, N. E., 'The response of a single-degree-of-freedom system with quadratic and cubic nonlinearities to a principal parametric resonance', *J. Sound Vib.* **129**, 1989, 417–442.
10. Nayfeh, A. H., *Perturbation Methods*, Wiley-Interscience, 1973.
11. Nayfeh, A. H., *Introduction to Perturbation Techniques*, Wiley-Interscience, 1981.
12. Zavodney, L. D. and Shihada, S. M., 'The role of damping in the suppression of parametric resonances in nonlinear systems', DAMPING 89, West Palm Beach, FL, February 8–10, 1989.
13. Szemplinska-Stupnicka, W., Plaut, R. H., and Hsieh, J. C., 'Period doubling and chaos in unsymmetric structures under parametric excitation', *J. Appl. Mech.* **56**, 1989, 947–952.
14. Nayfeh, A. H. and Sanchez, N. E., 'Chaos and dynamic instability in the rolling motion of ships', *Proceedings of the Seventeenth Symposium on Naval Hydrodynamics*, The Hague, The Netherlands, August 29–September 2, 1988, National Academy Press, 1989, 617–631.
15. Nayfeh, A. H. and Sanchez, N. E., 'Bifurcations in a forced softening Duffing oscillator', *Int. J. Nonl. Mech.* **24**, 1989, 483–497.